AIP | The Journal of Chemical Physics

Communication: Density-functional theory for inhomogeneous hyperbranched polymeric fluids: Polydisperse effect of degree of branching

Xiaofei Xu and Dapeng Cao

Citation: The Journal of Chemical Physics **133**, 121101 (2010); doi: 10.1063/1.3490794
View online: http://dx.doi.org/10.1063/1.3490794
View Table of Contents: http://scitation.aip.org/content/aip/journal/jcp/133/12?ver=pdfcov
Published by the AIP Publishing

Communication: Density-functional theory for inhomogeneous hyperbranched polymeric fluids: Polydisperse effect of degree of branching

Xiaofei Xu and Dapeng Cao[a)]
Division of Molecular and Materials Simulation, Key Laboratory for Nanomaterials, Ministry of Education, Beijing University of Chemical Technology, Beijing 100029, People's Republic of China

(Received 29 July 2010; accepted 25 August 2010; published online 28 September 2010)

We developed a new density-functional theory (DFT) for inhomogeneous hyperbranched polymers that is able to describe the polydisperse degree of branching quantitatively. The topological contributions of the polymer chains to the Helmholtz free energy take into account the effect of triple connections that are absent in previous DFT investigations. One key advantage of the new theory is that the computational cost shows only a linear relationship with the molecular weight (rather than an exponential relationship). The practical utility of the new DFT is illustrated by investigating colloidal stability in the presence of monodisperse and polydisperse hyperbranched polymers. © *2010 American Institute of Physics*. [doi:10.1063/1.3490794]

It is a scientific ambition to predict how the polymer architecture could be altered to modify physical properties. To explore the effect of molecular architecture on physical properties, it is necessary to clearly understand the behavior of polymers with complex architecture like hyperbranched polymers.[1–3] Hyperbranched polymers are treelike macromolecules with densely branched structure. A number of branching points make them a variety of unique properties, such as the high functionality of end groups and biocompatibility with natural protein.[2]

Hyperbranched polymers are characterized by their multibranched, three-dimensional architecture with a wide range of polydispersity in both molecular weight and the degree of branching (DOB).[1] In addition, the functional groups are distributed randomly throughout the branched architecture. These variables of architecture have huge implications not only for the final equilibrium properties of a product but also for kinetic properties in the melt. Theoretical and computational studies of such implications may lead to a better understanding of the relationship between the molecular structure and macroscopic properties of hyperbranched polymers. A satisfactory modeling needs to reproduce the systematic properties related to all architectures of hyperbranched polymers. However, the total number of all architectures for N-mers is of order $O(\alpha^N N^{-2.5})$ (the constant $\alpha=2.955\,76\cdots$), which is an extremely great number, particularly for the chains with high molecular weight.[4] Therefore, it remains a challenge to model such a polydisperse system quantitatively.

In previous statistical mechanics investigations, such as Brownian dynamics simulation and nonequilibrium molecular dynamics simulation, it is usually assumed that the hyperbranched polymers have regular architecture, or only macroscopic properties of homogeneous system were explored.[5–9] In the past decade, it has proved that classical density-functional theory (DFT) is a powerful theoretical tool for the treatment of nonuniform polymeric fluids and solutions.[10,11] The theory is rooted in quantum mechanics but shares mathematical similarity with a number of classical theories of statistical mechanics. It provides a unifying computational method to describe the microscopic structure and phase behavior of soft condensed matter. In this work, we developed a new DFT for hyperbranched polymers to explore the polydisperse effect of the DOB quantitatively.

We consider the hyperbranched polymers with polydisperse architectures in a good solvent. Each molecule is modeled as a coarse-grained chain. The functionality of end groups are assumed to be not more than 3, which limits the maximum bonds of monomers formed. The architectures are characterized by their DOB, which is defined as $\beta_i=(d_i-d_L)/(d_D-d_L)$, $i=1,2,\ldots$. $d_i=\Sigma_{j=1}^{N_i} g_i^j(g_i^j-1)/2$ is the number of triple connections, N_i is the number of monomers for single polymer chain, and g_i^j is the number of bonds connected to segment j in architecture i; d_L and d_D are the number of triple connections for linear and dendritic chains having the same molecular weights with architecture i. In Fig. 1, we give an example to illustrate how to count the number of triple connections. For the 8-mers shown in Fig. 1(a), there are seven triple connections, i.e., connections of "123," "124," "324," "245," "456," "567," and "678." The architectures can be partitioned by the equivalence relation of DOB. That is to say, two architectures are assumed to have equivalent effect on the behavior of system if their DOBs are the same, i.e., their number of triple connections are the same. For instance, the architectures shown in Figs. 1(b) and 1(c) are equivalent to the one in Fig. 1(a) because they all have seven triple connections. In each classification, we choose a specific architecture to represent the equivalent classification. All the specific architectures in each equiva-

[a)]Author to whom correspondence should be addressed. Electronic addresses: caodp@mail.buct.edu.cn and cao_dp@hotmail.com. FAX: 86-10-64427616.

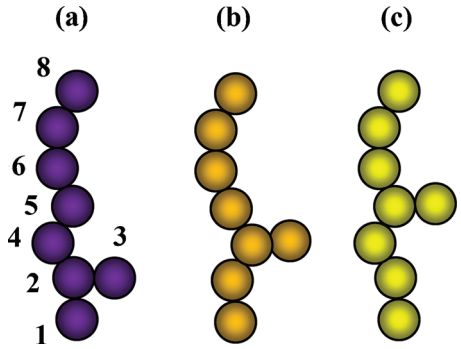

FIG. 1. Equivalent classification for 8-mers with seven triple connections.

lence classification of 22-mers used in this work are shown in Fig. 2.

Based on this assumption of equivalent classification, it just needs to consider the effect of the architectures with different DOBs. For N-mers, the total number of different DOBs is $[N/2]$, where $[\bullet]$ is the floor function. Thus, the number of the architectures to be considered exhibits a linear relation with the molecular weight, rather than the order of $O(\alpha^N N^{-2.5})$. For the polymers with high molecular weight, introduction of the DOB leads to a very significant simplification and saving computational efforts. The occurrence probability for the architectures in the polydisperse system is determined by the distribution of the DOBs. In this work, we construct it as follows:

$$P(\beta_i) \equiv P_i = K d_i^m \exp[-(m+1)d_i/d_b] \quad (i = 1,2,\ldots,s), \tag{1}$$

with $K=(\Sigma_{i=1}^{s} d_i^m \exp[-(m+1)d_i/d_b])^{-1}$. In Eq. (1), s is the total number of the architectures with different DOBs. d_b is the average number of triple connections for single chain in bulk phase. m determines the width of the distribution and the polydispersity index is defined as PDI$=(m+1)/m$. PDI $=1$ corresponds to monodisperse case. The larger the PDI, the more polydisperse is the polymer system.

In the scheme of DFT, the free energy for ideal polymer chain with architecture i is known exactly as

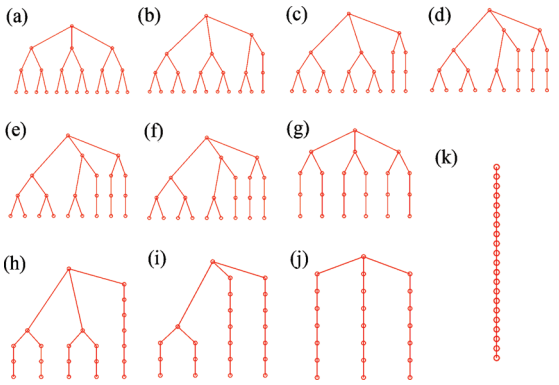

FIG. 2. The equivalent classifications of 22-mers. The numbers of triple connections are (a) 30, (b) 29, (c) 28, (d) 27, (e) 26, (f) 25, (g) 24, (h) 23, (i) 22, (j) 21, and (k) 20.

$$\beta F_i^{\mathrm{id}}[\rho_i(\boldsymbol{R})] = \int \mathrm{d}\boldsymbol{R}\rho_i(\boldsymbol{R})[\ln \rho_i(\boldsymbol{R}) - 1] + \beta \int \mathrm{d}\boldsymbol{R}\rho_i(\boldsymbol{R})V_i(\boldsymbol{R}), \tag{2}$$

where $\beta=1/(k_{\mathrm{B}}T)$ is the inverse thermal energy. The multipoint density profile $\rho_i(\boldsymbol{R})$ is a function of the chain configuration $\boldsymbol{R}=(\boldsymbol{r}_i^1,\ldots,\boldsymbol{r}_i^{N_i})$. The polymers are modeled as freely jointed chains, where neighboring monomers are bonded at a fixed separation σ. The intramolecular bonding constraints of the chain are described by the potential $V_i(\boldsymbol{R})$, which is given by $\exp[-\beta V_i(\boldsymbol{R})]=\Pi_{\substack{j_1\leftrightarrow j_2 \\ j_1<j_2}}\delta(|\boldsymbol{r}_i^{j_1}-\boldsymbol{r}_i^{j_2}|-\sigma)/(4\pi\sigma^2)$. $j_1\leftrightarrow j_2$ stands for the bond connecting segments j_1 and j_2, and δ is the Dirac function. For a polydisperse fluid, the total segmental density is defined as a summation of the monomeric density over every segment for all architectures, given by

$$\rho(\boldsymbol{r}) = \sum_{i=1}^{s}\sum_{j=1}^{N_i}\rho_i^j(\boldsymbol{r}) = \sum_{i=1}^{s}\int \mathrm{d}\boldsymbol{R}\sum_{j=1}^{N_i}\delta(\boldsymbol{r}-\boldsymbol{r}_i^j)\rho_i(\boldsymbol{R}). \tag{3}$$

In Eq. (3), $\rho_i^j(\boldsymbol{r})$ represents the segmental density of segment j of architecture i. The nonbonded interactions and the affiliated density correlation effects are accounted in the excess free energy, which is usually assumed to be a functional of total segmental density. For polymers in a good solvent considered in this work, the nonbonded interactions between polymer segments comprise of hard-sphere repulsion, and pair and triple chain connections. Thus, the excess free energy is

$$F^{\mathrm{ex}} = F_{\mathrm{hs}}^{\mathrm{ex}} + F_{\mathrm{pair}}^{\mathrm{ex}} + F_{\mathrm{triple}}^{\mathrm{ex}}. \tag{4}$$

The contribution $F_{\mathrm{hs}}^{\mathrm{ex}}$ from hard-sphere repulsion is given by a modified fundamental measure theory,[12,13] and the contribution $F_{\mathrm{pair}}^{\mathrm{ex}}$ from pair connection is described by the first order of thermodynamic perturbation theory (TPT1).[14]

TPT1 takes into account only the neighboring connections and neglects the topology of polymer chain completely.[15,16] To describe the behavior induced by the polydisperse architecture, the contribution from topology of polymer chain has to be included into the theory. Toward that end, it needs a reliable approximation for multiple correlation function of polymer chain, which is used as an input for the estimation of multi-interaction. Unfortunately, there is neither an analytical expression nor molecular simulation data available for the function of higher-order than three. Due to this restriction, in the contribution of polymer topology, the effect of triple connections is only taken into account. The excess free energy for triple connections is approximated by using TPT2.[16,17] By rewriting the functional in terms of Rosenfeld's weight density,[18] the free energy contribution from single triplet-connection for N-mers is

$$\phi_{\mathrm{triple}}^{\mathrm{chain}} = -\frac{1}{N} n_{0\mathrm{p}} \xi_{\mathrm{p}} \ln \Lambda[n_\alpha], \tag{5}$$

with

$$\Lambda[n_\alpha] = \int_0^\pi y_{\rm hs}^{(3)}[\sigma,\sigma,2\sigma\sin(\omega/2)]/[y_{\rm hs}^{(2)}(\sigma)]^2 B(\omega)\sin\omega d\omega, \tag{6}$$

where $y_{\rm hs}^{(3)}$ and $y_{\rm hs}^{(2)}$ are the triple and pair correlation functions for hard sphere, respectively. ω is the bond angle for the three consecutive segments in the triple connection. $B(\omega)$ describes the bond-angle distribution associated to the bending energy, which needs to satisfy the normalization condition. For a freely jointed chain, it is 2/3 at $\pi/3 \le \omega \le \pi$ and 0 at $0 \le \omega < \pi/3$. $n_\alpha(\alpha=0,1,2,3,V1,V2)$ are the weighted density defined by Rosenfeld. The triple correlation function can be approximated by the Percus–Yevick closure relation.[19,20] Based on this approximation, we derived the excess free energy accounting for all triple connections (averaged on every monomer), given by

$$F_{\rm triple}^{\rm ex}[\rho(\boldsymbol{r})] = -L\int {\rm d}\boldsymbol{r} n_{0\rm p}\xi_{\rm p}\ln\Lambda[n_\alpha], \tag{7}$$

where

$$\Lambda[n_\alpha] = (1 + an_2\sigma_{\rm p}\xi + bn_2^2\sigma_{\rm p}^2\xi)/(1-n_3)^3, \tag{8}$$

$$L = \left(\sum_{i=1}^{s}\beta_i P(\beta_i)/N_i\right) \Big/ \left(\sum_{i=1}^{s} P(\beta_i)N_i\right), \tag{9}$$

with $\xi_{\rm p} = 1 - \boldsymbol{n}_{\rm V2p}\cdot\boldsymbol{n}_{\rm V2p}/n_{2\rm p}^2$ and $\xi = 1 - \boldsymbol{n}_{\rm V2}\cdot\boldsymbol{n}_{\rm V2}/n_2^2$. The constants in Eq. (8) are $a=-2.7349$ and $b=1.6044$, which are obtained by fitting the equation of $y_{\rm hs}^{(3)}$ to the simulation data.[21]

In presence of an external potential $\psi(\boldsymbol{R})$ that acts on all monomers, the grand potential can be represented as

$$\Omega = \sum_{i=1}^{s} F_i^{\rm id}[\rho_i(\boldsymbol{R})] + F^{\rm ex}[\rho(\boldsymbol{r})] + \sum_{i=1}^{s}\int {\rm d}\boldsymbol{R}\rho_i(\boldsymbol{R})[\psi(\boldsymbol{R}) - \mu_i]. \tag{10}$$

In Eq. (10), μ_i is the chemical potential, given by $\beta\mu_i = \ln[\rho^b P(\beta_i)] + \beta\mu_i^{\rm ex}$. $\ln[\rho^b P(\beta_i)]$ is the ideal chemical potential, where ρ^b is the bulk density and $P(\beta_i)$ is the occurrence probability of architecture i. $\mu_i^{\rm ex}$ is the excess chemical potential, which is calculated from the expression of excess free energy functional in bulk phase. Minimization of Eq. (10) with respect to $\rho_i(\boldsymbol{R})$ gives the following s-equations:

$$\rho_i(\boldsymbol{R}) = \exp\left[\beta\mu_i - \beta V_i(\boldsymbol{R}) - \sum_{j=1}^{N_i}\lambda(r_j)\right], \quad i = 1,2,\ldots,s, \tag{11}$$

where $\lambda(\boldsymbol{r}_i) = \beta\varphi(\boldsymbol{r}_i) + \delta\beta F^{\rm ex}/\delta\rho(\boldsymbol{r}_i)$. According to our previous algorithm,[22–24] any polymer chains can be represented by a treelike structure containing root and leaf segments, which connects the segments by parent-child relation. Following this representation and combining Eq. (3), we obtain the segmental densities

$$\rho_{i,j}(\boldsymbol{r}) = \exp[\beta\mu_j - \beta\lambda(\boldsymbol{r})]G_j^{{\rm P}|i}(\boldsymbol{r})\prod_{\alpha={\rm child}(j)} G_j^{{\rm C}|i,\alpha}(\boldsymbol{r}), \quad 1 \le j \le N_i, \tag{12}$$

where the parent and child recursive functions are given by

$$G_{j\,[{\rm parent}(j)=k]}^{{\rm P}|i}(\boldsymbol{r}) = \begin{cases} 1, & j \text{ is root} \\ \dfrac{1}{4\pi\sigma^2}\displaystyle\int_{|r-r'|=\sigma}\exp[-\beta\lambda_k(\boldsymbol{r}')]G_k^{{\rm P}|i}(\boldsymbol{r}')\prod_{\substack{\alpha={\rm child}(k)\\ \alpha\neq i}} G_k^{{\rm C}|i,\alpha}(\boldsymbol{r}'){\rm d}\boldsymbol{r}', & j \text{ is not root,} \end{cases} \tag{13a}$$

$$G_{j\,[\alpha={\rm child}(j)]}^{{\rm C}|i,\alpha}(\boldsymbol{r}) = \begin{cases} \dfrac{1}{4\pi\sigma^2}\displaystyle\int_{|r-r'|=\sigma}\exp[-\beta\lambda_\alpha(\boldsymbol{r}')]\prod_{\beta={\rm child}(\alpha)} G_\alpha^{{\rm C}|i,\beta}(\boldsymbol{r}'){\rm d}\boldsymbol{r}', & j \text{ is not a leaf} \\ 1, & j \text{ is a leaf.} \end{cases} \tag{13b}$$

Equations (3), (12), and (13) form a closed set of s-equations to be solved self-consistently. The excess functional is constructed in the way that couples the contributions from all architectures [see Eq. (7)]. It should be mentioned that the functional can also be built by separately treating each architecture. In that way, the resulting functional has to solve s-equations, which leads to an extremely large time-consumption. On the contrary, the numerical implementation of the coupled functional [Eq. (7)] is quite efficient because only one equation needs to be solved in this case. For polymers with high molecular weight, the coupled way would present a significant computational time-saving, even for the systems with quite wide distribution of DOBs.

Here, we also illustrate the application of this new polymer DFT by exploring the effect of polydispersity on colloidal stability. We consider two "large" colloidal particles im-

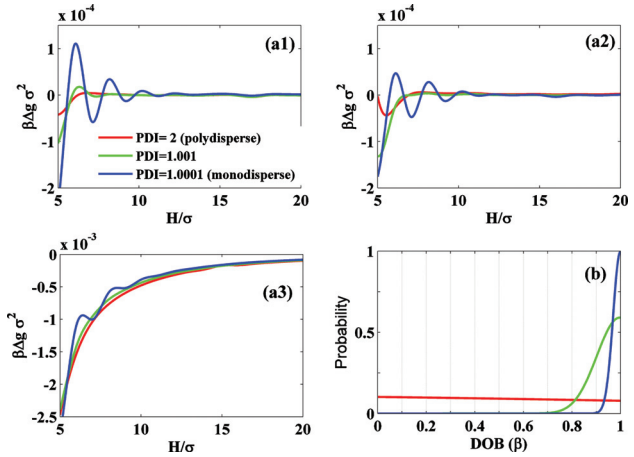

FIG. 3. (a) The polydisperse effect of degree of branching for 22-mers on the interaction energy of surfaces at $\eta_b=0.01$. The strength of the surface attraction are (1) $a_w=0$, (2) $a_w=0.5$, and (3)$a_w=0.7$. (b) The probability distribution of DOBs used in the calculation.

mersed in a sea of hyperbranched polymers with polydisperse architectures. The colloids are modeled as two flat and parallel surfaces of infinite area, perpendicular to the z direction and located at $z=0$ and $z=H$. The interaction between the surfaces and monomers is given by Lennard-Jones potential $w(z)=\varepsilon[(2/15)(\sigma/z)^9-a_w(\sigma/z)^3]$. An adsorbing surface is characterized by $a_w>0$, while $a_w=0$ creates a nonadsorbing surface. The solvent molecules are modeled as monomeric hard spheres, which interact with the surface by a hard wall potential. The particle-particle interactions are athermal to mimics the conditions of good solvents. The good solubility of polymers in these solvents gives rise to effective repulsive interactions between monomers. The interaction energy per unit area is defined as $\Delta g(H)=g(H)-g(\infty)$, where $g(H)=\Omega_{\text{eq}}/S+P_bH$. Here, S is the surface area, P_b is the bulk pressure, and Ω_{eq} is the equilibrium grand potential. If $\Delta g(H)>0$, the interaction between the two surfaces is repulsive, whereas if $\Delta g(H)<0$, the interaction is attractive. The bulk DOB used in this work is $\beta_b=1$.

In Fig. 3(a), we study the polydisperse effect of DOB on the interaction energy per unit area between both adsorbing and nonadsorbing surfaces. As is shown, the polydisperse effect is quite drastic. For nonadsorbing surfaces [see Fig. 3(a)(1)], the interaction in monodisperse case (PDI =1.0001) at small separation H presents an oscillatory barrier between attraction and repulsion. Because monodisperse polymers have consistent radius of gyration, the packing way strongly depends on the separation H and leads to the oscillatory barrier. As the PDIs increase to 1.001 and 2, the oscillatory barrier is absent and a monotonic attractive interaction is presented due to the influx of the chains of various radii of gyration into the region between surfaces. In this case, the packing way is tighter than the monodisperse case, and is independent on the surface separation, which therefore diminishes the oscillatory barrier, and induces the attractive interaction due to the depletion effect. Similar behavior is also observed in the case of adsorbing surfaces [Fig. 3(a)(2) and Fig. 3(a)(3)]. The oscillatory barrier also appears in monodisperse case, while it disappears as the PDI increases. However, unlike the case of nonadsorbing surfaces, the oscillatory barriers decrease in the polydisperse case due to the bridging effect of the influx linear chains. Linear chains are longer than hyperbranched chain and may bridge the two surfaces to induce an attractive interaction.[25]

In conclusion, we have developed a new DFT for inhomogeneous hyperbranched polymers, which is able to describe the polydisperse effect of DOB quantitatively. Importantly, the topological contributions of polymer chains are included into the Helmholtz free energy by taking into account the effect of triple connections. Furthermore, the approach can be easily applied to most other versions of polymer DFTs. Another advantage of this approach is that its time-consuming shows a linear relationship with the molecular weight rather than an exponential relationship. Accordingly, it is particularly useful on treating more complex problems requiring integrals of higher dimensionality.

This work was supported by the NSF of China (Grant Nos. 20874005 and 20736002), the National Basic Research Program (Grant No. 2011 CB 706900) and the Novel Team (Grant No. IRT 0807) from Ministry of Education, and the "Chemical Grid Project" and Excellent Talents Funding of BUCT. We are greatly thankful to Professor J. Z. Wu from UC Riverside for his constructive suggestion and comments.

[1] D. Wilms, S. E. Stiriba, and H. Frey, Acc. Chem. Res. **43**, 129 (2010).
[2] W. D. Jang, K. M. K. Selim, C. H. Lee, and I. K. Kang, Prog. Polym. Sci. **34**, 1 (2009).
[3] M. Ujihara and T. Imae, Polym. Int. **59**, 137 (2010).
[4] R. Otter, Ann. Math. **49**, 583 (1948).
[5] D. Konkolewicz, R. G. Gilbert, and A. Gray-Weale, Phys. Rev. Lett. **98**, 238301 (2007).
[6] F. Jasch, C. von Ferber, and A. Blumen, Phys. Rev. E **68**, 051106 (2003).
[7] A. Blumen, A. Jurjiu, T. Koslowski, and C. von Ferber, Phys. Rev. E **67**, 061103 (2003).
[8] T. C. Le, B. D. Todd, P. J. Daivis, and A. Uhlherr, J. Chem. Phys. **130**, 074901 (2009).
[9] J. T. Bosko and J. R. Prakash, J. Chem. Phys. **128**, 034902 (2008).
[10] J. Z. Wu, *Molecular Therodynamics of Complex Systems* (Springer-Verlag, Berlin, 2009), Vol. 131, pp. 1–73.
[11] J. Z. Wu, AIChE J. **52**, 1169 (2006).
[12] Y. X. Yu and J. Z. Wu, J. Chem. Phys. **117**, 10156 (2002).
[13] R. Roth, R. Evans, A. Lang, and G. Kahl, J. Phys.: Condens. Matter **14**, 12063 (2002).
[14] D. P. Cao and J. Z. Wu, J. Chem. Phys. **121**, 4210 (2004).
[15] M. S. Wertheim, J. Stat. Phys. **42**, 477 (1986).
[16] M. S. Wertheim, J. Chem. Phys. **87**, 7323 (1987).
[17] S. Phan, E. Kierlik, M. L. Rosinberg, H. Yu, and G. Stell, J. Chem. Phys. **99**, 5326 (1993).
[18] Y. Rosenfeld, Phys. Rev. Lett. **63**, 980 (1989).
[19] P. Attard, J. Chem. Phys. **91**, 3072 (1989).
[20] E. A. Müller and K. E. Gubbins, Mol. Phys. **80**, 91 (1993).
[21] E. A. Müller and K. E. Gubbins, Mol. Phys. **80**, 957 (1993).
[22] X. F. Xu, D. P. Cao, X. R. Zhang, and W. C. Wang, Phys. Rev. E **79**, 021805 (2009).
[23] X. F. Xu and D. P. Cao, J. Chem. Phys. **130**, 164901 (2009).
[24] X. F. Xu and D. P. Cao, J. Chem. Phys. **131**, 054901 (2009).
[25] D. P. Cao and J. Z. Wu, Langmuir **22**, 2712 (2006).